ESC European Society of Cardiology

Cardiovascular Research (2022) **118**, 2610–2624
https://doi.org/10.1093/cvr/cvab306

Temporal relationship between systemic endothelial dysfunction and alterations in erythrocyte function in a murine model of chronic heart failure

Tasnim Mohaissen [1,2], Bartosz Proniewski [1], Marta Targosz-Korecka[3], Anna Bar [1], Agnieszka Kij [1], Katarzyna Bulat [1], Aleksandra Wajda [1,4], Aneta Blat [1,4], Karolina Matyjaszczyk-Gwarda [1,2], Marek Grosicki [1], Anna Tworzydlo [1], Magdalena Sternak [1], Kamila Wojnar-Lason [1,5], Raquel Rodrigues-Diez [6,7], Agata Kubisiak[3], Ana Briones [6,7], Katarzyna M. Marzec [1], and Stefan Chlopicki [1,5]*

[1]Jagiellonian University, Jagiellonian Center for Experimental Therapeutics (JCET), 14 Bobrzynskiego St., 30-348 Krakow, Poland; [2]Jagiellonian University Medical College, Faculty of Pharmacy, 9 Medyczna St., 30-688, Krakow, Poland; [3]Jagiellonian University Medical College, Faculty of Physics, Institute of Astronomy and Applied Computer Science, 11 Lojasiewicza St., 30-348 Krakow, Poland; [4]Jagiellonian University, Faculty of Chemistry, 2 Gronostajowa St., 30-387 Krakow, Poland; [5]Jagiellonian University Medical College, Faculty of Medicine, Chair of Pharmacology, 16 Grzegorzecka St., 31-531 Krakow, Poland; [6]Universidad Autónoma de Madrid, Instituto de Investigación Hospital Universitario La Paz (IdiPaz), Departamento de Farmacología, Facultad de Medicina, C/Arzobispo Morcillo 4, Madrid, 28029, Spain; and [7]Centro de Investigación Biomédica en Red de Enfermedades Cardiovasculares (CIBERCV), C/Arzobispo Morcillo 4, 28029, Madrid, Spain

Received 18 February 2021; editorial decision 12 September 2021; online publish-ahead-of-print 7 October 2021

Time for primary review: 31 days

This manuscript was handled by Consulting Editor Ajay M. Shah.

Aims Endothelial dysfunction (ED) and red blood cell distribution width (RDW) are both prognostic factors in heart failure (HF), but the relationship between them is not clear. In this study, we used a unique mouse model of chronic HF driven by cardiomyocyte-specific overexpression of activated Gαq protein (Tgαq*44 mice) to characterize the relationship between the development of peripheral ED and the occurrence of structural nanomechanical and biochemical changes in red blood cells (RBCs).

Methods and results Systemic ED was detected *in vivo* in 8-month-old Tgαq*44 mice, as evidenced by impaired acetylcholine-induced vasodilation in the aorta and increased endothelial permeability in the brachiocephalic artery. ED in the aorta was associated with impaired nitric oxide (NO) production in the aorta and diminished systemic NO bioavailability. ED in the aorta was also characterized by increased superoxide and eicosanoid production. In 4- to 6-month-old Tgαq*44 mice, RBC size and membrane composition displayed alterations that did not result in significant changes in their nanomechanical and functional properties. However, 8-month-old Tgαq*44 mice presented greatly accentuated structural and size changes and increased RBC stiffness. In 12-month-old Tgαq*44 mice, the erythropathy was featured by severely altered RBC shape and elasticity, increased RDW, impaired RBC deformability, and increased oxidative stress (gluthatione (GSH)/glutathione disulfide (GSSG) ratio). Moreover, RBCs taken from 12-month-old Tgαq*44 mice, but not from 12-month-old FVB mice, coincubated with aortic rings from FVB mice, induced impaired endothelium-dependent vasodilation and this effect was partially reversed by an arginase inhibitor [2(S)-amino-6-boronohexanoic acid].

Conclusion In the Tgαq*44 murine model of HF, systemic ED accelerates erythropathy and, conversely, erythropathy may contribute to ED. These results suggest that erythropathy may be regarded as a marker and a mediator of systemic ED in HF. RBC arginase and possibly other RBC-mediated mechanisms may represent novel therapeutic targets for systemic ED in HF.

*Corresponding author. Tel: +48 12 6645464; fax: +48 12 2974615, E-mail: stefan.chlopicki@jcet.eu

Graphical Abstract

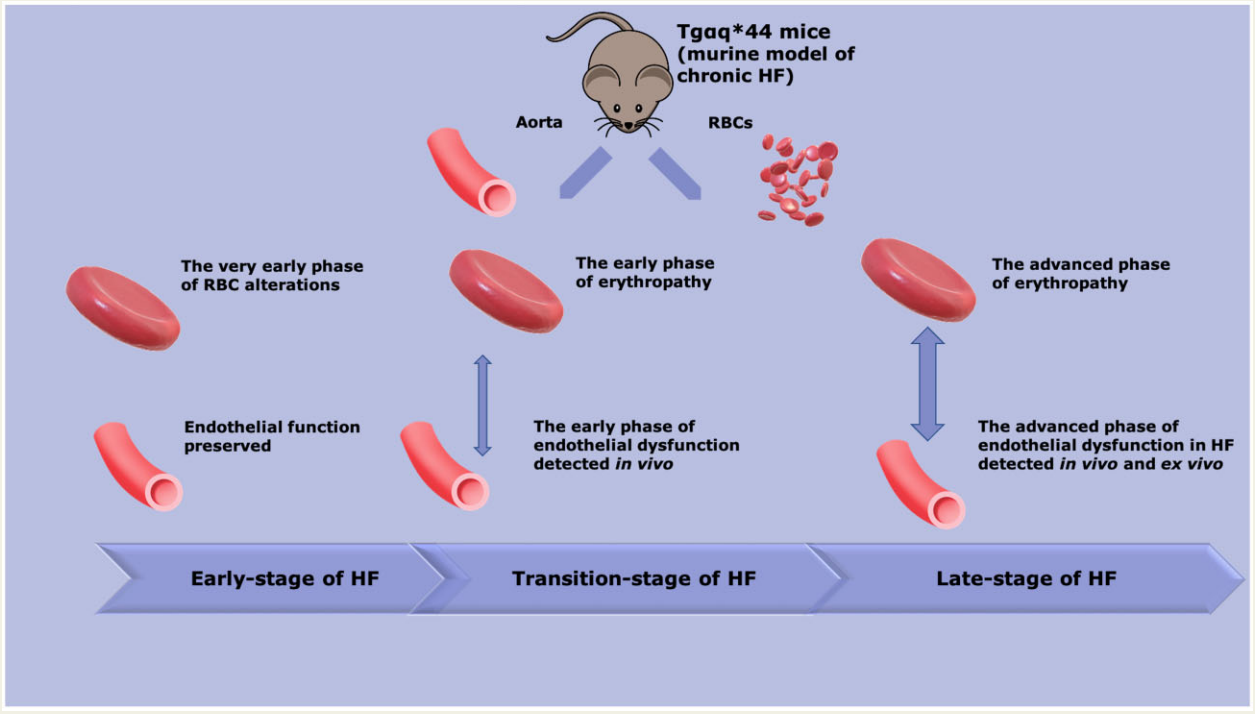

Keywords Heart failure • Endothelial dysfunction • Red blood cells • Erythropathy

1. Introduction

Heart failure (HF) is an outcome of various primary and secondary incidents; in the advanced stage, it results not only in impaired cardiac function but also in the development of endothelial dysfunction (ED) in the peripheral circulation[1] as well as alterations in red blood cell (RBC) function.[2] However, the relationship between ED and the functional, structural, nanomechanical, and biochemical properties of RBCs in HF is not clear.

In various diseases, including HF, ED is characterized by impaired production of nitric oxide (NO) and increased production of superoxide ($O_2^{\bullet -}$)[1] as well as other changes in the endothelial phenotype.[1,3] Consistent with the oxidative stress-related mechanisms of ED, antioxidant treatment strategies, including vitamin C and NADPH oxidase 2 and xanthine oxidase inhibitors, have been shown to improve endothelial function in HF.[4–6] Various mechanisms of peripheral ED have been proposed, including a decrease in shear stress linked to cardiac failure, which leads to the downregulation of endothelial nitric oxide synthase (eNOS) expression and the reduction of NO production alongside increased oxidative stress.[3,7] Several contributors to ED in HF have been proposed: neurohormonal activation, with major roles of angiotensin II (Ang II)[3,8] and mineralocorticoid receptor (MR)-dependent mechanisms;[7] hyperactivation of the sympathetic system;[1,9] and proinflammatory cytokines, including tumour necrosis factor alpha (TNFα) and interleukin (IL)-6.[1] Notably, the most effective pharmacological treatments for HF patients, such as renin–angiotensin system (RAS) inhibitors, which include angiotensin-converting enzyme (ACE) inhibitors,[10] Ang II type 1 receptor antagonists,[8] and MR antagonists,[11] improved endothelial function in the peripheral circulation of HF patients. Improvement in peripheral ED by RAS-based treatment strategies and other treatment strategies has therapeutic benefits for HF,[10] including increased exercise tolerance in HF patients.[12]

ED in peripheral circulation may have prognostic value independent of whether the HF is ischaemic or non-ischaemic.[13] However, although abundant literature exists related to peripheral ED in HF of ischaemic origin,[3,14] little is known about the mechanism of ED in non-ischaemic HF. Indeed, some[3,15] but not all[3,16] authors have confirmed the development of ED in HF of non-ischaemic origin.

Interestingly, although RBCs display physiological size heterogeneity, increased red blood cell distribution width (RDW) is an independent predictor of the short- and long-term prognosis of HF,[17,18] implicating the role of altered function of RBCs in the pathophysiology of HF. Several reciprocal mechanisms between the endothelium and RBCs maintain the haemostatic balance and safeguard the cardiovascular system, whereas alterations of this balance may lead to vascular pathologies such as ED.[19] For example, functional alterations in RBCs induced by hyperglycaemia, diabetes,[19] a high-fat diet,[20] malaria, and haemoglobinopathies (e.g. sickle cell diseases) contribute to the pathomechanisms of ED,[19] and various mechanisms have been proposed for these RBC functional changes.[21,22]

Despite the knowledge that ED and RDW are both prognostic factors in HF, the relationship between alterations in RBC function and the development of peripheral ED in HF is not clear. Although patients with HF present alterations in several haemorheological properties as well as

impairment of peripheral blood flow,[23] it is not known whether these pathologies are related, whether they occur simultaneously, or whether one precedes the other. To the best of our knowledge, the link between RBC alterations and endothelial function in HF has not been defined previously.

To fill this gap, we characterized the development of peripheral ED and the progression of functional, structural, nanomechanical, and biochemical alterations of RBCs, taking advantage of a unique murine model of chronic heart failure (CHF) generated by cardiomyocyte-specific overactivation of the Gαq protein (Tgαq*44 mice), which imitates excessive neurohormonal cardiac activation.[24] This model is relevant to the pathophysiology of human HF and is characterized by prolonged HF progression, with distinct early and late stages of the disease that have been described previously.[25,26] Thus, this model seemed well suited to characterize the temporal associations between alterations in endothelial and RBC function, two phenomena involved in HF pathophysiology.

2. Methods

2.1. Animals

Female Tgαq*44 mice, a model of HF initially developed by Mende *et al.*,[24,27] and FVB (wild-type) mice were bred in the Animal Laboratory of the Medical Research Centre of the Polish Academy of Sciences (Warsaw, Poland). Tgαq*44 mice based on the FVB strain express an HA epitope-tagged, constitutively active mutated αq (HAα*q) under the control of the α-MHC promoter and represent a unique model of CHF.[24,27] All animal procedures were in accordance with the Guide for the Care and Use of Laboratory Animals published by the US National Institutes of Health (NIH Publication No. 85-23, revised 1985) as well as with the local ethical committee on Animal Experiments in Krakow. Mice were fed a standard chow diet and kept in 12:12 light–dark conditions.

2.2 Assessment of endothelium-dependent vasodilation and endothelial permeability *in vivo* by magnetic resonance imaging

Endothelial function and permeability *in vivo* were assessed as described previously.[28–30] Briefly, endothelium-dependent vasodilation *in vivo* was assessed by measuring the response to acetylcholine (Ach, Sigma-Aldrich, Poznań Poland: 50 µL, 16.6 mg/kg, i.p.) in the abdominal aorta (AA) and by flow-mediated dilatation (FMD) in response to reactive hyperaemia (after 5 min vessel occlusion) in the femoral artery (FA).[29] Changes in endothelial function were expressed as changes in the vessel volume.[30] Moreover, changes in endothelial permeability were assessed by relaxation time (T_1) map measurements in the brachiocephalic artery (BCA) using the variable flip angle technique[31,32] before and 30 min after intravenous (i.v.) administration of a unique formulation of gadolinium contained in the liposome [gadodiamide in the liposome, concentration of formulation: (287 mg/mL, 4.5 mL/kg, i.v.)] as described before.[28,29]

2.3 Aorta isolation

Mice were euthanized intraperitoneally with a mixture of ketamine and xylazine in doses of 100 and 10 mg/kg body weight, respectively. Subsequently, the aorta was removed and placed in cold Krebs–Henseleit solution (KB) bubbled with a 95% O_2/5% CO_2 mixture (pH = 7.4). Aortic segments used for NO, superoxide, or eicosanoid production were immediately placed in fresh KB or frozen at -80°C.

2.3.1 Assessment of endothelium-dependent and -independent vasodilation *ex vivo* in wire myograph system

Aortic rings were mounted in a Mulvany myograph system (620 M, Danish Myo Technology, Denmark), followed by assessment of the endothelium-dependent and independent vasodilation *ex vivo*, carried out as previously described.[33] To study RBC-induced ED, RBCs from 12-month-old Tgαq*44 or 12-month-old FVB mice were isolated,[34] diluted with serum-free culture medium to a haematocrit (HCT) of 5%, and were incubated with aortic rings isolated from 12-month-old Tgαq*44 or 12-month-old FVB mice in cell culture incubator at 37°C with 5% carbon dioxide for 18 h in the absence or presence of 100 µM of 2(S)-amino-6-boronohexanoic acid (ABH).

2.3.2 Assessment of eicosanoid production in isolated aortic rings by liquid chromatography coupled to mass spectrometry (LC–MS/MS)

Aortic rings were added to a 24-well plate containing KB. The plate was placed into a BIO-V gas treatment chamber (Noxygen Science, Elzach, Germany), where it remained for 15 min under CO_2 flow at 37°C. After pre-incubation, the aortic rings were placed into 500 µL of fresh KB, and 100 µL samples of the incubation buffer were taken after 3 and 45 min of incubation. The concentrations of 6-keto prostaglandin F1α (6-keto $PGF_{1\alpha}$), as well as prostaglandin E_2 and D_2 (PGE_2 and PGD_2) and 15-hydroxyeicosatetraenoic acid (15-HETE) in the aorta effluents, were examined by a liquid chromatograph UFLC Nexera (Shimadzu, Kyoto, Japan) coupled to a triple quadrupole mass spectrometer QTRAP 5500 (SCIEX, Framingham, MA, USA) following the methodology previously described.[35] The biosynthesis of prostacyclin (PGI_2) and thromboxane A_2 (TXA_2) were assessed based on the concentration of their stable metabolites 6-keto $PGF_{1\alpha}$ and thromboxane B_2 (TXB_2), respectively. Results are presented as the difference between the concentration assessed after 3 and 45 min incubation.

2.3.3 Assessment of NO and $O_2^{\bullet -}$ production in the isolated aorta by electron paramagnetic resonance spectroscopy

NO production in the isolated aorta was measured by electron paramagnetic resonance (EPR) with the cell-permeable NO spin trapping agent diethyldithiocarbamate (DETC), as described previously.[36]

2.3.4 Assessment of TNFα and IL-1β gene expression by quantitative reverse transcriptase real-time PCR (qRT-PCR)

Total RNA was extracted from the aorta of Tgaq*44 and FVB mice with TRI Reagent (Sigma-Aldrich, St. Louis, MO, USA) following the manufacturer's procedures, as described previously.[37]

2.4 Blood and RBC analysis

Depending on the applied method of analysis; the blood samples, isolated RBCs or RBC membranes were studied. Whole blood samples were collected from the right ventricle using a syringe containing additional anticoagulant (heparin). The details of RBC isolation from the whole blood and RBC membrane isolation (prepared by overnight freezing of RBCs suspended in 0.9% NaCl, HCT = 10%) are presented in the Supplementary material online.

2.4.1 Blood count, blood biochemistry, and determination of NO metabolites

A whole blood sample was used for blood count analysis using an automatic haematology analyser ABC Vet (Horiba, Kyoto, Japan). Plasma obtained after centrifugation (acceleration: 1000 × *g*, run time: 10 min, 4°C) was used for measuring the lipid profile with an ABX Pentra biochemical analyser (Horiba Medical Kyoto, Japan).

Measurement of nitrate (NO_3^-) and nitrite (NO_2^-) concentrations in the plasma was performed using an ENO-20 NOx analyser (Eicom Corp., Kyoto, Japan), applying a liquid chromatography method with post-column derivatization using Griess reagent, as previously described.[38] The packed RBCs remaining after centrifugation were used for gluthatione (GSH) and glutathione disulfide (GSSG) concentration measurement as well as nitrosyl haemoglobin (HbNO) detection with EPR spectroscopy.[38,39]

2.4.2 Assessment of RBC shape and nanomechanics by atomic force microscopy(AFM)

Erythrocyte shape and elasticity were measured using a NanoWizard 3 (JPK Instruments, Berlin, Germany) AFM microscope. All measurements were performed using a pyramidal AFM probe attached to V-shaped silicon nitride cantilevers with a spring constant of 0.01 N/m (MLCT-C, Veeco Probes, Camarillo, CA, USA). The force mapping mode was used for both topography and elasticity measurements. The elastic moduli of RBCs were calculated using the Hertz–Sneddon model with the approximation for a paraboloidal probe. Data were analysed using JPKSPM Data Processing software. The aspect ratio was defined as the ratio between two perpendicular main axes of the RBCs (i.e. the length and width of the cell).[40]

2.4.3 Assessment of RBC deformability by RheoScan

Erythrocyte deformability was measured using a microfluidic RheoScan AnD 300 (RheoMeditech, Seoul, South Korea) following the protocol suggested by the manufacturer. RBC deformation was quantified at a shear stress of 20 Pa in terms of the maximum elongation index.[40]

2.4.4 Assessment of RBC by flow cytometry

RBCs and reticulocytes were analysed with a BD LSR II flow cytometer (BD Biosciences, Oxford, UK) and stained against anti-mouse TER-119 PerCP/Cy5.5 (BioLegend, San Diego, CA, USA) and anti-mouse CD71 APC (BioLegend) antibodies and annexin V FITC (antibody dilution 1:100, stained for 30 min at room temperature). For each sample 100 000 000 events were acquired in log mode for forward side scatter (SSC), SSC, and fluorescent signals. Data were analysed using BD FACSDiva Software (BD Biosciences). RBC and reticulocytes were gated according to their characteristic log FCS, log SSC, and fluorescent signals.

2.4.5 Assessment of GSH and GSSG concentration in RBCs by capillary electrophoresis

GSH and GSSG concentrations were measured using a P/ACE MDQ capillary electrophoresis system (Beckman Coulter, Fullerton, CA, USA) with 32 Karat software (ver. 8.0, Beckman Coulter) as previously described.[41]

2.4.6 Assessment of biochemical content of RBC membranes by Raman spectroscopy and Fourier transform infrared spectroscopy–attenuated total reflectance

Isolated RBC membranes were deposited on CaF2 slides, air-dried for 30 min, and examined with Raman spectroscopy (RS) followed by Fourier transform infrared spectroscopy (FTIR)–attenuated total reflectance, as previously described.[40,42]

Details of methods are given in Supplementary material online.

2.5 Statistical analysis

Statistical analyses were performed using GraphPad Prism 8.4 (GraphPad Software). The results are presented as box plots (median, Q1, Q3, interquartile range, and outliers). Tgαq*44 mice in different phases of HF were compared with age-matched control groups and analysed using two-way ANOVA. The normality of the distribution and homogeneity of variance were tested using the Shapiro–Wilk and *F*-tests, respectively. When these assumptions were violated, non-parametric tests were performed (Kruskal–Wallis ANOVA). Probability values (*P*) of <0.05 were considered statistically significant.

3. Results

3.1 Development of systemic ED in Tgαq*44 mice, *in vivo* magnetic resonance imaging-based measurements

Magnetic resonance imaging (MRI)-based assessment of endothelium-dependent response *in vivo* revealed that in 8-month-old Tgαq*44 mice, Ach-induced vasodilation in the AA was impaired, whereas in older mice (10- to 12-month-old Tgαq*44 mice), Ach-induced vasodilation was completely lost and changed to vasoconstriction (*Figure* 1A, $P < 0.05$). ED in 8-month-old Tgαq*44 mice was confirmed by increased endothelial permeability measured *in vivo* by MRI with the use of the Npx50 parameter of endothelial permeability.[28] The T_1 signal near the BCA lumen after i.v. injection of gadolinium-containing liposomes was increased in Tgαq*44 mice aged 8 months and older compared with age-matched FVB mice (*Figure 1B*). In contrast, flow-mediated vasodilation (FMD) in the FA was fully preserved in 8-month-old Tgαq*44 mice compared with that in age-matched FVB mice. FMD in the FA was also slightly impaired in 12-month-old Tgαq*44 mice, but this difference did not reach statistical significance (*Figure 1C*).

3.2 Development of ED in the aorta of Tgαq*44 mice; *ex vivo* measurements

In 10- and 12-month-old Tgαq*44 mice, but not in 6- and 8-month-old Tgαq*44 mice, Ach-induced endothelium-dependent vasodilation was decreased compared with the age-matched FVB mice (*Figure 1D–G*), whereas endothelium-independent vasodilation induced by sodium nitroprusside (SNP) was fully preserved in all experimental groups of Tgαq*44 mice and age-matched FVB mice (*Figure 1H–K*).

3.3 Systemic bioavailability of NO in Tgαq*44 mice

Systemic ED in Tgαq*44 mice was not associated with a reduction in the NO_2^- concentration in plasma. However, the NO_3^- plasma concentration decreased in 10- to 12-month-old Tgαq*44 mice compared with that of FVB mice (*Table 1*). In contrast to the lack of decreased plasma NO_2^-

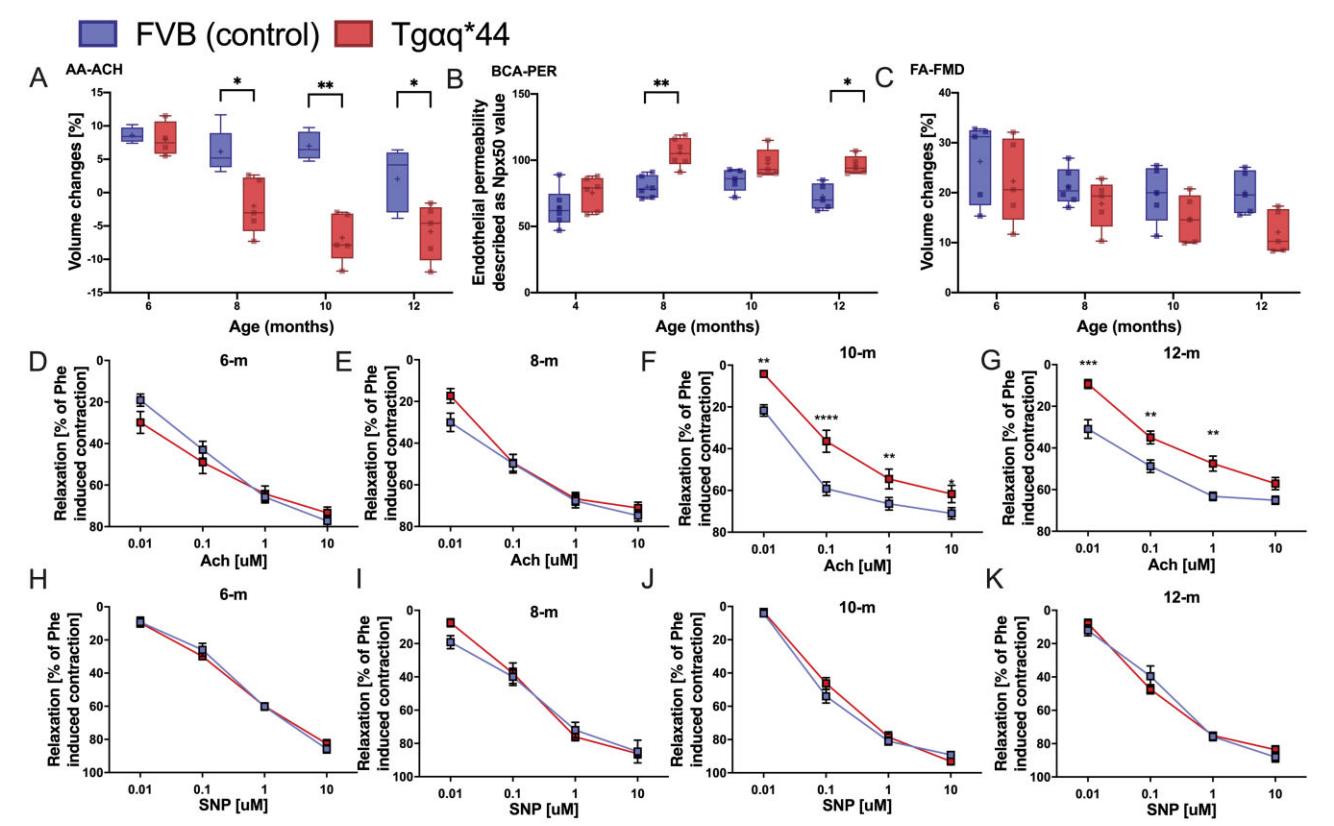

Figure 1 Peripheral vascular endothelial dysfunction with the progression of HF in Tgαq*44 mice compared with age-matched FVB mice. *In vivo* changes in the end-diastolic volume of the abdominal aorta 25 min after Ach administration ($n = 4–6$) (*A*). Changes in endothelial permeability described as Npx50 value, after injection of gadolinium-rich liposome contrast agent (brachiocephalic artery permeability BCA-PER) ($n = 5–6$) (*B*). *In vivo* changes in the volume of the femoral artery in response to flow-mediated vasodilation (FA-FMD) after 5-min vessel occlusion ($n = 5–6$) (*C*). *Ex vivo*: Relaxation of the aorta rings in response to increasing doses of Ach (*D–G*) and SNP (*H–K*) ($n = 6–8$) in 4-, 8-, 10-, and 12-month-old Tgαq*44 mice vs. age-matched FVB control mice. Normality was assessed using a Shapiro–Wilk test. Results are presented as box plots (median, Q1, Q3, whiskers indicate minimum/maximum), Q1 and Q3 indicate the 25th and 75th percentiles, respectively (*A–C*), mean ± SEM (*D–K*). $^{*}P < 0.05$, $^{**}P < 0.01$, $^{***}P < 0.001$ $^{****}P < 0.0001$, Tgαq*44 mice and age-matched FVB control mice compared using two-way ANOVA with *post hoc* Sidak test. SNP, sodium nitroprusside.

concentration, the HbNO content in RBCs substantially decreased in 12-month-old Tgαq*44 mice compared with that in the RBCs of age-matched FVB mice (*Table 1*). Tgαq*44 mice did not display any changes in blood biochemistry compared with age-matched FVB mice until the age of 12 months, when the plasma concentration of the urea significantly increased, whereas the total cholesterol and HDL cholesterol plasma levels modesty decreased in Tgαq*44 mice compared with the levels in FVB mice (*Table 1*).

3.4 Alterations in NO/$O_2^{\bullet-}$ balance and in eicosanoid production in the aorta of Tgαq*44 mice

ED in the aorta of 12-month-old Tgαq*44 mice was accompanied by a decrease in stimulated NO production in *ex vivo* aortas measured by EPR (*Figure 2A*) compared with age-matched FVB mice. Furthermore, impairment of endothelial functional response in the aorta was associated with increased $O_2^{\bullet-}$ production in 12-month-old Tgαq*44 mice compared with that in age-matched FVB (*Figure 2B*).

In 12-month-old Tgαq*44 mice, but not in younger Tgαq*44 mice, the production of 6-keto $PGF_{1\alpha}$, PGE_2, PGD_2, and 15-HETE in the aorta was higher than in age-matched FVB mice (*Figure 2C–F*). However, TNFα (*Figure 2G*) and IL-1β (*Figure 2H*) mRNA gene expression in the aorta did not differ between the 12-month-old Tgαq*44 mice and age-matched FVB mice.

3.5 Basic characterization of alterations in RBCs in Tgαq*44 mice

Alterations in RBC indices were not associated with significant differences in haemoglobin, HCT, or white blood cell and platelet (PLT) counts between Tgαq*44 mice and age-matched FVB mice (*Table 1*). Mean corpuscular haemoglobin (MCH) and MCH concentration (MCHC) were lower in 8- to 12-month-old Tgαq*44 mice than in age-matched FVB mice, but not in the early stage of HF (*Table 1*), whereas mean corpuscular volume (MCV) was significantly lower in 4- to 12-month-old Tgαq*44 mice than in age-matched FVB mice (*Figure 3A*). RDW was significantly increased in 10- to 12-month-old Tgαq*44 mice (*Figure 3B*) compared with that in age-matched FVB mice. There was no statistically significant difference in the extent of reticulocytosis between Tgαq*44 and FVB mice (*Figure 3C*). The annexin V staining did not differ between Tgαq*44 and FVB mice at the age of 4 months and was slightly decreased

Table 1 Body mass, blood count, lipid profile, and NO metabolism in Tgαq*44 mice compared with age-matched FVB mice

	4 months		8 months		10 months		12 months	
	FVB	Tgαq*44	FVB	Tgαq*44	FVB	Tgαq*44	FVB	Tgαq*44
Body mass (g)	24.21 ± 1.47	25.309 ± 1.391	27.28 ± 2.46	28.65 ± 2.28	29.49 ± 2.46	30.95 ± 3.08	29.95 ± 2.90	26.83 ± 2.1*
Biochemical parameters								
TC (mmol/L)	2.680 ± 0.271	3.019 ± 0.366	2.41 ± 0.29	2.84 ± 0.66	2.97 ± 0.28	2.6 ± 0.42	3.21 ± 0.28	2.51 ± 0.26*
HDL (mmol/L)	1.07 ± 0.11	1.263 ± 0.192	0.97 ± 0.14	1.18 ± 0.24	1.31 ± 0.09	1.12 ± 0.20	1.33 ± 0.137	1.04 ± 0.13*
LDL (mmol/L)	0.2 ± 0.02	0.197 ± 0.021	0.2 ± 0.06	0.18 ± 0.08	0.20 ± 0.03	0.19 ± 0.03	0.19 ± 0.02	0.2 ± 0.03
TG (mmol/L)	2.03 ± 0.42	2.581 ± 0.847	3.02 ± 0.780	2.73 ± 1.485	2.76 ± 0.357	2.839 ± 0.568	2.59 ± 0.364	2.921 ± 1.128
Creatinine (μmol/L)	20.16 ± 3.93	18.471 ± 2.766	21.31 ± 3.76	17.62 ± 3.65	19.2 ± 3.63	20.69 ± 2.31	19.23 ± 2.95	24.97 ± 5.49
Urea (mmol/L)	6.77 ± 2.06	7.753 ± 0.99	8.50 ± 0.73	8.84 ± 1.12	8.49 ± 1.47	8.41 ± 2.23	8.15 ± 1.41	12.50 ± 1.42**
Blood count								
WBC (K/μL)	3.61 ± 0.659	3.291 ± 1.075	4.02 ± 1.254	4.02 ± 1.701	3.24 ± 0.821	3.59*±0.9453	2.77 ± 0.785	3.33 ± 1.08
PLT (K/μL)	1209.85 ± 102.25	1244.273 ± 95.289	1159.08 ± 120.86	1298.75 ± 160.3	1050 ± 174.018	1285.92*±212.7394	1217.17 ± 81.13	1345.58 ± 157.29
RBC (M/μL)	9.59 ± 0.413	10.081 ± 0.448	9.811 ± 0.246	9.851 ± 0.330	10.420 ± 0.812	10.26 ± 0.675	9.18 ± 0.66	9.66 ± 0.60
HGB (g/dL)	14.21 ± 0.705	14.455 ± 0.611	14.91 ± 0.434	14.3 ± 0.47	15.61 ± 1.081	14.46 ± 0.85	14.47 ± 0.819	13.72 ± 0.82
HCT (%)	52.284 ± 2.388	54.2 ± 2.603	54.133 ± 1.444	53.1 ± 1.82	56.882 ± 4.177	53.93 ± 3.55	50.65 ± 3.61	51.47 ± 2.97
MCHC (g/dL)	27.185 ± 0.40	26.67 ± 0.41	27.53 ± 0.72	26.89 ± 0.39*	27.42 ± 0.41	26.59 ± 0.23**	28.29 ± 0.42	26.65 ± 0.27****
No metabolism								
NO_2^- (μM)	2.09 ± 0.46	2.03 ± 0.51	1.21 ± 0.52	1.20 ± 0.18	1.48 ± 0.39	1.16 ± 0.42	1.03 ± 0.37	1.04 ± 0.49
NO_3^- (μM)	30.71 ± 11.23	30.63 ± 8.85	14.70 ± 10.09	11.22 ± 2.91	23.66 ± 8.14	11.90 ± 3.72*	23.46 ± 3.96	10.41 ± 3.83*
HbNO (arb u)	602.85 ± 117.14	448.06 ± 54.994*	335.35 ± 135.2	230.62 ± 103.19	461.629 ± 135.39	362.659 ± 123.26	505.967 ± 189.09	226.959 ± 79.75***

*Body mass ($n = 9–13$), blood biochemistry ($n = 7$): TC, total cholesterol; HDL, high-density lipoprotein; LDL, low-density lipoprotein; TG, triglycerides; creatinine, and urea. Blood count ($n = 9–13$): WBC, white blood cells; PLT, platelets; RBC, red blood cells; HGB, haemoglobin; HCT, haematocrit; MCH, mean corpuscular haemoglobin; MCHC, mean corpuscular haemoglobin concentration. NO metabolism ($n = 5–13$): Nitrite (NO_2), Nitrate (NO_3^-) concentration, HbNO, nitrosyl haemoglobin in 4-, 8-, 10-, and 12-month-old Tgαq44 mice vs. age-matched FVB controls mice. Normality was assessed using a Shapiro–Wilk test. Results are presented as means ± SD. Tgαq*44 mice and age-matched FVB controls compared using two-way ANOVA with *post hoc* Sidak test or non-parametric Kruskal–Wallis test (NO_2^- and NO_3^-).

*$P < 0.05$,

**$P < 0.01$,

***$P < 0.001$,

****$P < 0.0001$.

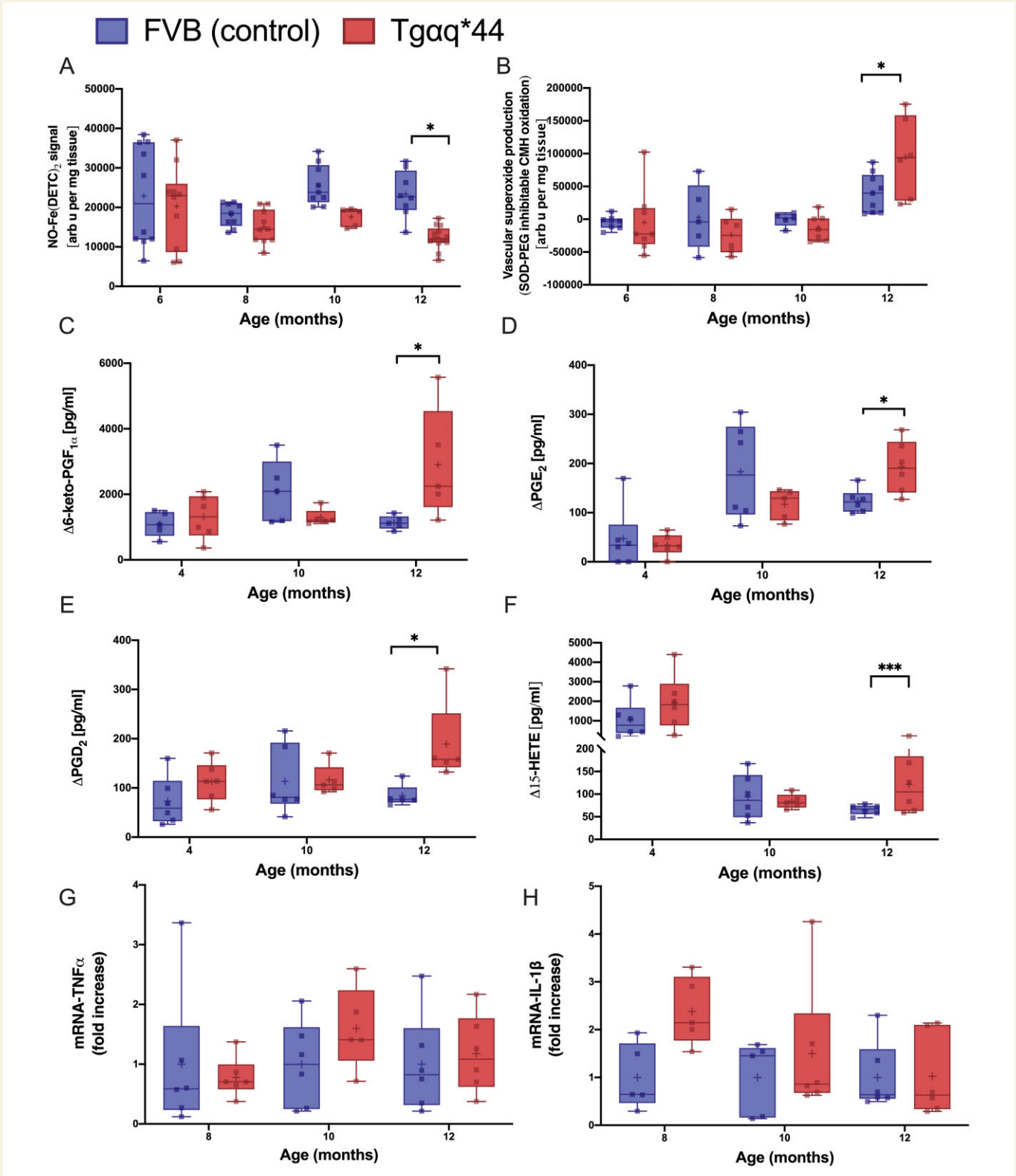

Figure 2 Alterations in NO/superoxide balance, eicosanoid, TNFα and IL-1β gene expression in the aorta with the progression of HF in Tgαq*44 mice compared with age-matched FVB mice. NO production in the isolated aorta ($n = 5–13$) (*A*), $O_2^{\bullet-}$ production in aortic rings ($n = 5–13$) (*B*), basal production of eicosanoid ($n = 5–6$) 6-keto $PGF_{1\alpha}$ (*C*), PGE_2 (*D*), PGD_2 (*E*), and 15-HETE (*F*) detected in the effluent after 45 min of incubation of isolated aortic rings. TNF (*G*) and IL-1β (*H*) gene expression ($n = 5–6$) in the aorta in 4-, 8-, 10-, and 12-month-old Tgαq*44 mice vs. FVB controls. Normality was assessed using a Shapiro–Wilk test. Results are presented as box plots (median, Q1, Q3, whiskers indicate minimum/maximum). Q1 and Q3 indicate the 25th and 75th percentiles, respectively. *$P < 0.05$, **$P < 0.01$, ***$P < 0.001$, ****$P < 0.0001$, Tgαq*44 mice compared with age-matched FVB controls using two-way ANOVA with *post hoc* Sidak test. ; IL-1β, interleukin-1β; NO, nitric oxide; TNFα, tumour necrosis factor alpha.

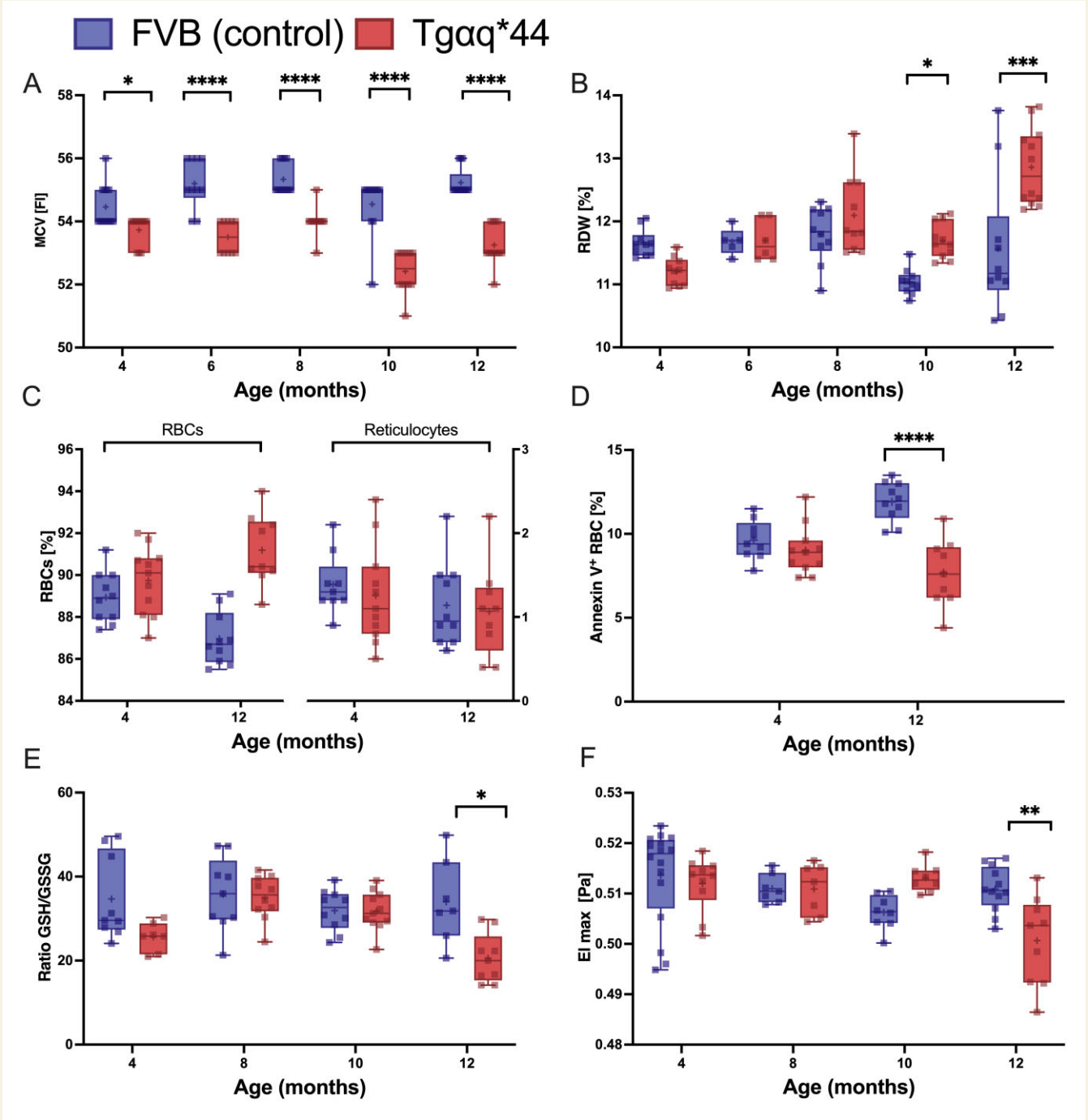

Figure 3 Alteration in blood count, apoptotic RBCs, GSH/GSSG ratio (oxidative stress), and erythrocyte deformability with the progression of HF in Tgαq*44 mice compared with age-matched FVB mice. The MCV ($n = 11–12$) (*A*) and RDW ($n = 10–12$) (*B*) in the blood in 4-, 6-, 8-, 10-, and 12-month-old Tgαq*44 mice vs. FVB controls mice. The percentage of RBCs and reticulocytes ($n = 9–11$) (*C*), and the number of apoptotic RBCs ($n = 9–11$) (*D*) in the blood samples in 4- and 12-month-old Tgαq*44 mice vs. FVB mice. The glutathione redox ratio ($GSSG{\cdot}GSH^{-1}$) ($n = 7–10$) (*E*), RBCs deformability ($n = 7–12$) (*F*) at shear stress (20 Pa) in the RBCs in 4-, 8-, 10-, and 12-month-old Tgαq*44 mice vs. FVB controls mice. Normality was assessed using a Shapiro–Wilk test. Results are presented as box plots (median, Q1, Q3, whiskers indicate minimum/maximum). Q1 and Q3 indicate the 25th and 75th percentiles, respectively. $^{*}P < 0.05$, $^{**}P < 0.01$, $^{***}P < 0.001$, $^{****}P < 0.0001$, Tgαq*44 mice compared with age-matched FVB controls using two-way ANOVA with *post hoc* Sidak test. ; MCV, mean corpuscular volume; RBC, red blood cell; RDW, red blood cell distribution width.

in 12-month-old Tgαq*44 mice compared with that in age-matched FVB mice (*Figure 3D*).

Total glutathione, GSH, and GSSG in RBCs did not show statistically significant differences between Tgαq*44 mice and FVB mice (data not shown), but the GSH/GSSG ratio was significantly lower in 12-month-old Tgαq*44 mice compared with that in age-matched FVB mice (*Figure 3E*). RBC deformability measured at a high shear stress (20 Pa) displayed a marked decrease in 12-month-old

Tgαq*44 mice compared with that in age-matched FVB mice (*Figure 3F*).

3.6 Characterization of alterations in topography and nanomechanics of RBCs in Tgαq*44 mice by AFM

The examples of RBC images in *Figure 4* reflect high variability of RBC shape during HF progression, from a normal biconcave shape to discocytes and spherocytes with irregular symmetry. In the control sample from 4-month-old FVB mice, a characteristic biconcave or doughnut shape of RBCs was observed. In 12-month-old FVB mice (*Figure 4B*), the deformation of the blood cells was manifested by a slight loss of symmetry in the height of the blood cells. In Tgαq*44 mice, more pronounced changes in RBC shape were observed (*Figure 4C–H*). In the youngest mice, a change in the shape of the RBCs was manifested either by an increase in the central part of the blood cell or a large change in the RBC height profile symmetry. In 8-month-old Tgαq*44 mice, significant cell deformation resulting in aspect ratio modification and diminished biconcave shape were noted. These changes were even more pronounced in 12-month-old Tgαq*44 mice.

The quantitative results of the aspect ratio are presented in *Figure 5A*, and the measured cell elastic moduli are presented in *Figure 5B*. In 8-, 10-, and 12-month-old Tgαq*44 mice, both parameters were significantly increased compared with the parameters in age-matched control mice. In 4- and 6-month-old Tgαq*44 mice, the differences did not reach statistical significance. Interestingly, there was a significant negative correlation between endothelial function (measured *in vivo* by MRI) and RBC elasticity (measured by AFM) in Tgαq*44 mice, and this correlation was not observed in FVB mice (*Figure 5C*). As shown in *Figure 5D-F*, the increased RBC aspect ratio was correlated with increased stiffness in both Tgaq*44 and FVB mice along with ageing; however, Tgaq*44 mice displayed a marked shift towards a higher aspect ratio and a higher elastic moduli value.

3.7 Effects of RBCs isolated from Tgαq*44 mice during early and end-stage HF on endothelium-dependent vasodilation, *ex vivo* measurements

As shown in *Figure 5G*, RBCs isolated from 12-month-old Tgαq*44 mice that were coincubated with aortic rings induced the impairment of endothelium-dependent vasodilation, whereas endothelial-independent vasodilation was preserved (Figure 5H). In contrast, RBCs isolated from 12-month-old FVB mice did not impair the endothelial function in the aortic rings. Interestingly, in the presence of ABH (100 μM), an inhibitor of arginase, the detrimental effect of RBCs taken from 12-month-old Tgαq*44 mice on endothelial function in the aorta was prevented. The effect of ABH was significant only for the highest concentration of Ach (10 μM), but there were no effects of ABH on SNP-induced relaxation (*Figure 5I and J*).

3.8 Characterization of alterations in biochemical contents of RBC membranes in Tgαq*44 mice by vibrational spectroscopy

In the RBC membranes of Tgαq*44 mice compared with age-matched FVB mice, FTIR-based analysis revealed that stretching

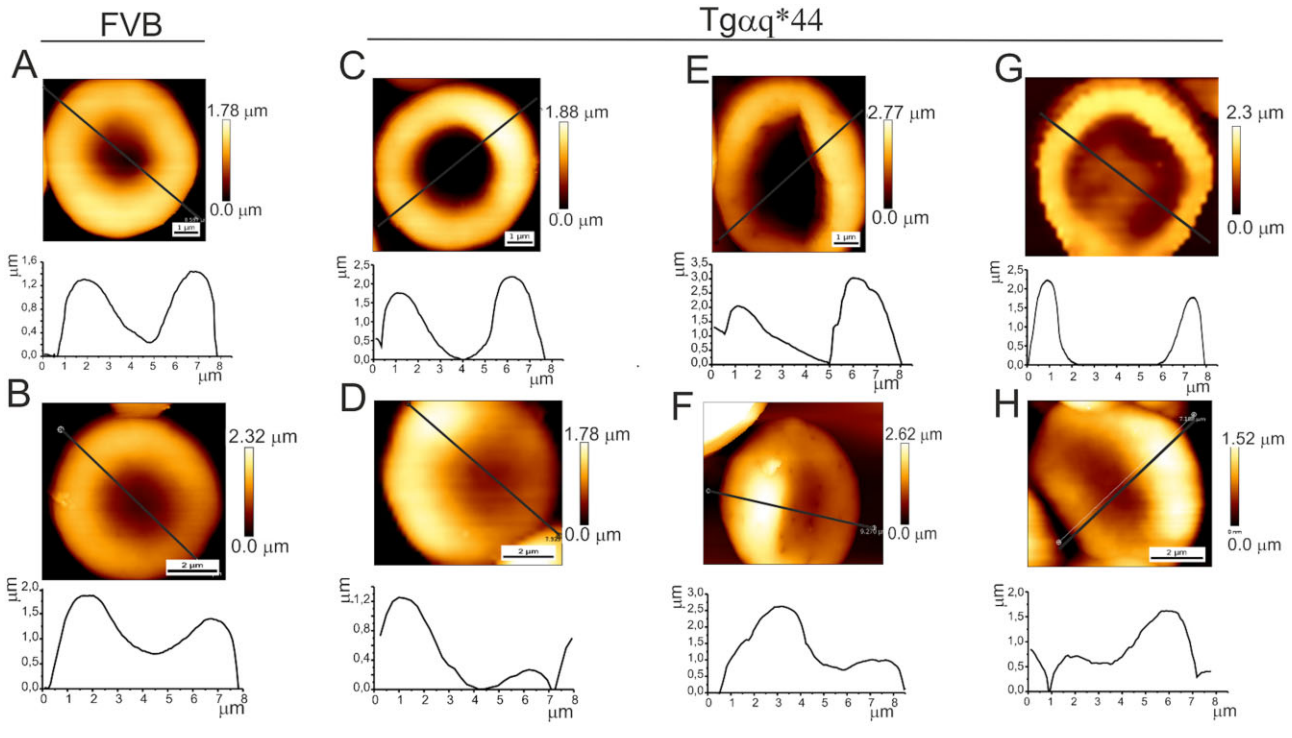

Figure 4 Variability of RBC shape along the progression of HF in Tgαq*44 mice compared with age-matched FVB mice. Examples of RBC images taken for 4-month-old (*A*) and 12-month-old (*B*) FVB mice (control sample). Examples of RBC shape changes observed for 4-month-old (*C and D*), 8-month-old (*E and F*), and 12-month-old (*G and H*) Tgαq*44 mice. Plots below AFM images show cross-sections along the marked lines. FVB, •••.

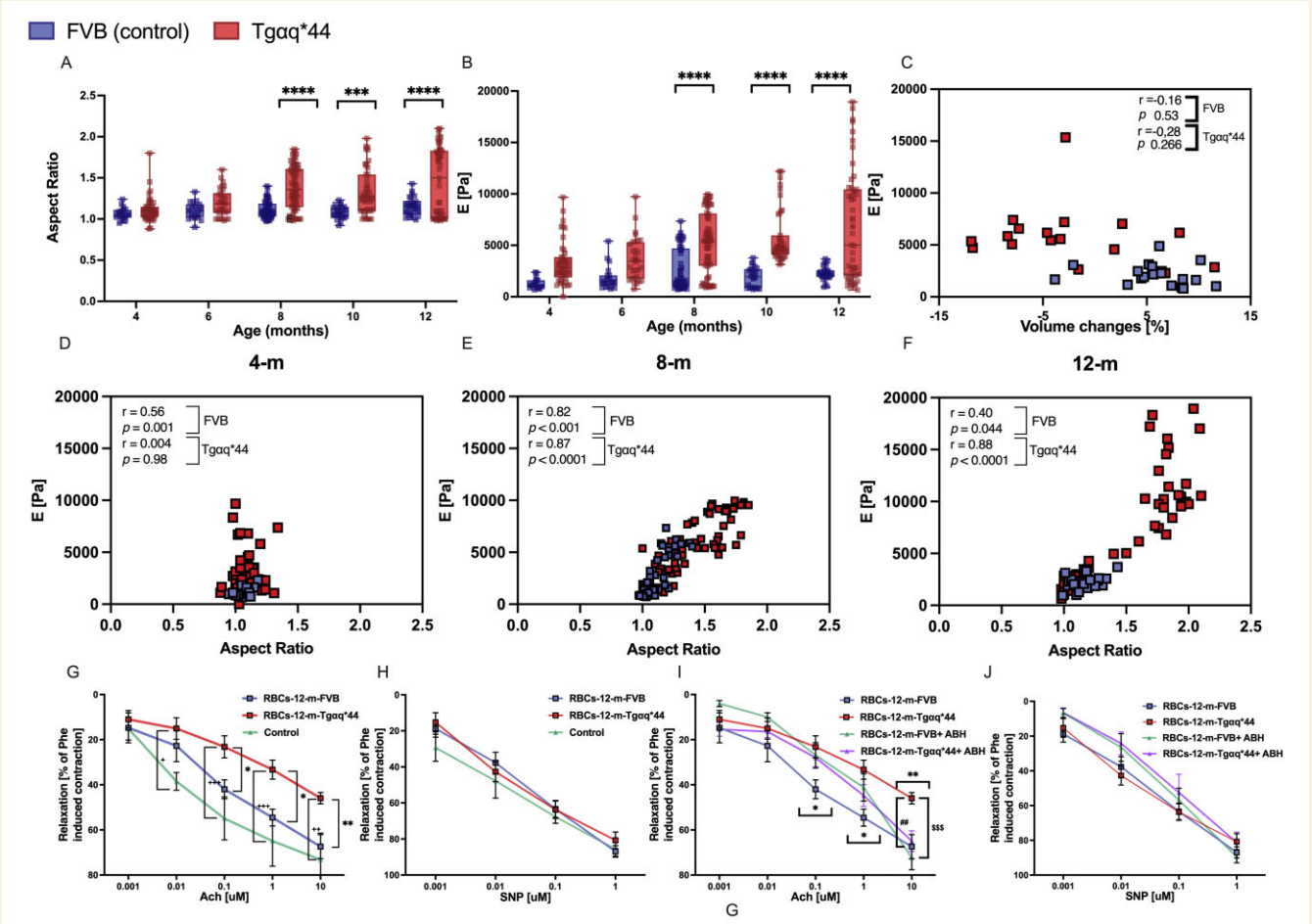

Figure 5 Changes in the aspect ratio and elastic moduli of RBCs with the progression of HF in Tgαq*44 mice compared with age-matched FVB mice (*A*–F). Effects of RBC coincubation with the aorta on endothelium-dependent relaxation (G–J). Cell aspect ratio of RBCs ($n = 5$–6, 6 repeats per mouse) (*A*), elastic modulus of RBCs ($n = 5$–6, 6 repeats per mouse) (*B*), correlation between elasticity modulus in RBCs and ED (*C*), correlation between aspect ratio and elasticity modulus in RBCs in 4- (D), 8- (E) and 12-(F) month-old Tgαq*44 mice vs. FVB control mice. Endothelium-dependent relaxation induced by ACh (G) and endothelium-independent relaxation induced by SNP (H) in the aortas isolated from 4-month-old FVB mice coincubated with RBCs isolated from 12-month-old Tgαq*44 mice (RBCs-12-m-Tgαq*44) or 12-month-old FVB mice (RBCs-12-m-FVB) ($n = 5$–6). Effects of 2(S)-amino-6-boronohexanoic acid (ABH, 100 μm) on responses to Ach (I) and SNP (J) in the aortas isolated from 4-month-old FVB mice coincubated with RBCs isolated from 12-month-old Tgαq*44 mice (RBCs-12-m-Tgαq*44) or 12-month-old FVB mice (RBCs-12-m-FVB) (n = 5–6). Normality was assessed using a Shapiro–Wilk test. Results are presented as box plots (median, Q1, Q3, whiskers indicate minimum/maximum), Q1 and Q3 indicate the 25th and 75th percentiles, respectively (*A and B*), mean ± SEM (G–J). $^{*}P < 0.05$, $^{**}P < 0.01$, $^{***}P < 0.001$, $^{****}P < 0.0001$, Tgαq*44 mice compared with age-matched FVB controls, $^{+}P < 0.05$, $^{++}P < 0.01$, $^{+++}P < 0.001$, Control vs. RBCs-12-m-Tgαq*44, $^{\$\$\$}P < 0.001$ RBCs-12-m-Tgαq*44 vs. RBCs-12-m-FVB-ABH, $^{\#\#}P < 0.01$ RBCs-12-m-Tgαq*44 vs. RBCs-12-m-Tgαq*44-ABH using two-way ANOVA with *post hoc* Sidak test.; RBC, red blood cell; SNP, sodium nitroprusside.

vibrations of the =CH groups (band at 3013 cm^{-1}) and antisymmetric stretching vibrations of the PO_2^- groups (band at 1235 cm^{-1}) differed significantly, indicating a reduction in phospholipid content (*Figure 6A*) and a decrease in the unsaturation of membrane lipids (*Figure 6D*). These changes were statistically significant in 4-month-old Tgαq*44 mice compared with FVB mice, and a similar degree of difference was observed in 12-month-old Tgαq*44 mice compared with FVB mice. RS and FTIR did not reveal changes in proteins fraction (*Figure 6C*), total lipids to proteins ratio (*Figure 6E*) or the fraction of esters (*Figure 6F*), including cholesterol esters (*Figures 6B* in RBC membranes obtained from 4- and 12-month-old Tgαq*44 compared with age-matched FVB mice.

4. Discussion

In the present work, we used a comprehensive methodology to assess the endothelial and RBC functional status and characterize the temporal relationships between the development of ED and the development of erythropathy in Tgαq*44 mice, a unique murine model of CHF with a prolonged time course of the HF progression. In contrast to most animal models, in which the transition from compensated to uncompensated CHF is relatively rapid, the Tgαq*44 murine model is characterized by a delayed progression to end-stage HF.[24–26,44] The prolonged window of HF progression in Tgαq*44 mice from adaptive to end-stage HF allowed us to discover that RBC alterations occurred very early in HF pathophysiology and progressed substantially with HF progression. In particular,

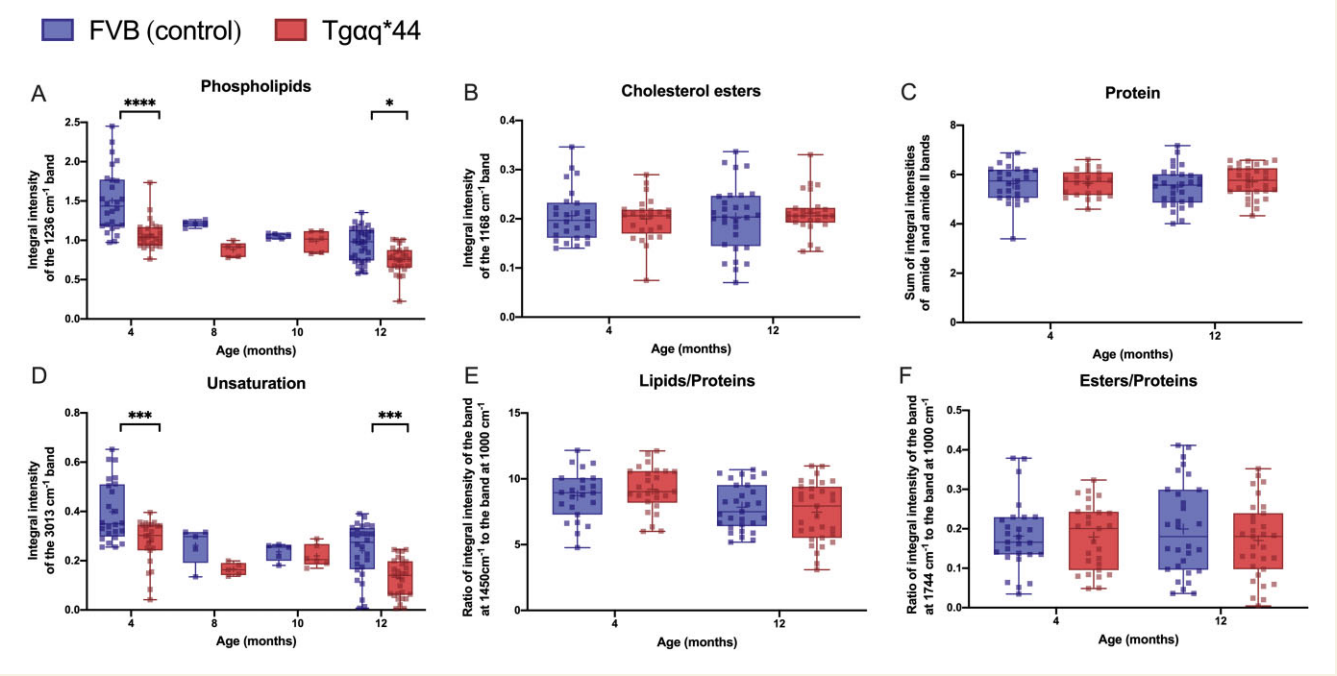

Figure 6 Changes of biochemical components of RBC membranes with the progression of HF in Tgαq*44 mice compared with age-matched FVB mice. The integration regions for IR bands: phospholipids (*A*) at 1236 cm^{-1} (1269–1194 cm^{-1}), cholesterol esters (*B*) at 1168 cm^{-1}(1182-1141cm^{-1}), proteins (*C*) as sum of amide I (1672–1608 cm^{-1}) and amide II (1562–1503 cm^{-1}), unsaturation (*D*) at 3013 cm^{-1} (3001–2980 cm^{-1}). Ratios of the integral intensities of RS bands: at 1450 cm^{-1} to 1000 cm^{-1} representing lipid/protein ratio (*E*), at 1744 cm^{-1} to 1000 cm^{-1} representing ester/protein ratio (*F*). $N = 5–6$ mice per experiment (total $n = 32–36$) for 4- and 12-month-old mice. In 8- and 10-month-old mice, one independent experiment was carried out on pooled RBCs obtained from $n = 12$ mice per group (5 average spectra from randomly measured points: 30 for RS and 5 for IR). Normality was assessed using a Shapiro–Wilk test. Results are presented as box plots (median, Q1, Q3, whiskers indicate minimum/maximum), Q1 and Q3 indicate the 25th and 75th percentiles, respectively. $^{*}P < 0.05$, $^{**}P < 0.01$, $^{***}P < 0.001$, $^{****}P < 0.0001$, Tgαq*44 mice compared with age-matched FVB controls, two-way ANOVA with *post hoc* Sidak test.

HF-linked erythropathy in Tgαq*44 mice accelerated substantially and was correlated with the progression of systemic ED. Increased RBC stiffness assessed by AFM was correlated with impaired endothelial function assessed *in vivo* by MRI. Finally, RBCs in late-stage erythropathy induced ED when coincubated with aorta samples from FVB mice, whereas RBCs in early erythropathy stages did not. These results suggest a possible reciprocal relationship between RBC alterations and endothelial function in HF: systemic ED accelerates erythropathy and, conversely, erythropathy may contribute to ED. Such a reciprocal relationship was previously postulated to occur in other diseases[19] but was not previously characterized in HF.

The major advantage of our experimental approach was that we assessed endothelial function by the application of an MRI-based method *in vivo*, a method that was validated in our previous studies.[28,29,43] This approach appeared to be more sensitive for detecting the early phase of ED (in 8-month-old Tgαq*44 mice) compared with classical isolated vessel studies *ex vivo* (in 10-month-old Tgαq*44 mice) and the direct measurement of NO/$O_2^{\bullet-}$ balance (in 12-month-old Tgαq*44 mice). Using our comprehensive methodological approach, we demonstrated that systemic ED was present in 8-month-old Tgαq*44 mice (impaired Ach-induced vasodilation and increased endothelial permeability *in vivo*) and progressed further in 10-month-old Tgαq*44 mice, as evidenced by impaired Ach-induced vasodilation with preserved SNP response in the aorta *ex vivo*. Furthermore, in 12-month-old Tgαq*44 mice, impaired NO production and increased $O_2^{\bullet-}$ production, phenomena that have been reported previously in HF,[3–5] were observed through biochemical measurements of the aorta.

Interestingly, in contrast to the impaired endothelial function in the aorta, the flow-mediated vasodilation in the femoral artery (FMD response in the FA) *in vivo* seemed to be largely preserved until end-stage HF. Previous studies have demonstrated heterogeneity in the response of the aorta and the FA in ageing and diabetes[45,46] As age increased, relaxation in response to Ach was reduced in the aorta, whereas in the FA response was fully preserved.[47] In addition, in db/db mice, the vasodilatory response to Ach was impaired in the FA but not in the aorta.[48] Finally, in a model of HF induced by myocardial infarction[45,46] FMD in the FA was heavily impaired, while the response to Ach was only moderately affected. Comparing the results of these studies with our findings underscores the heterogeneous response of the endothelium to HF progression in the conduit vessels in ischaemic and non-ischaemic HF and reveals a difference in response depending on the vascular bed and stimulus used.[46,49]

Interestingly, impaired Ach-induced NO-dependent vasodilation in the aorta was associated with a progressive reduction in plasma concentration of nitrate (8- to 12-month-old Tgαq*44 mice), whereas the concentration of nitrite remained unchanged, which suggests the activation of the nitrate–nitrite–NO reductive pathway, an alternative compensatory source that maintains NO bioavailability.[2] However, as the HbNO content in RBCs substantially decreased in 12-month-old Tgαq*44 mice

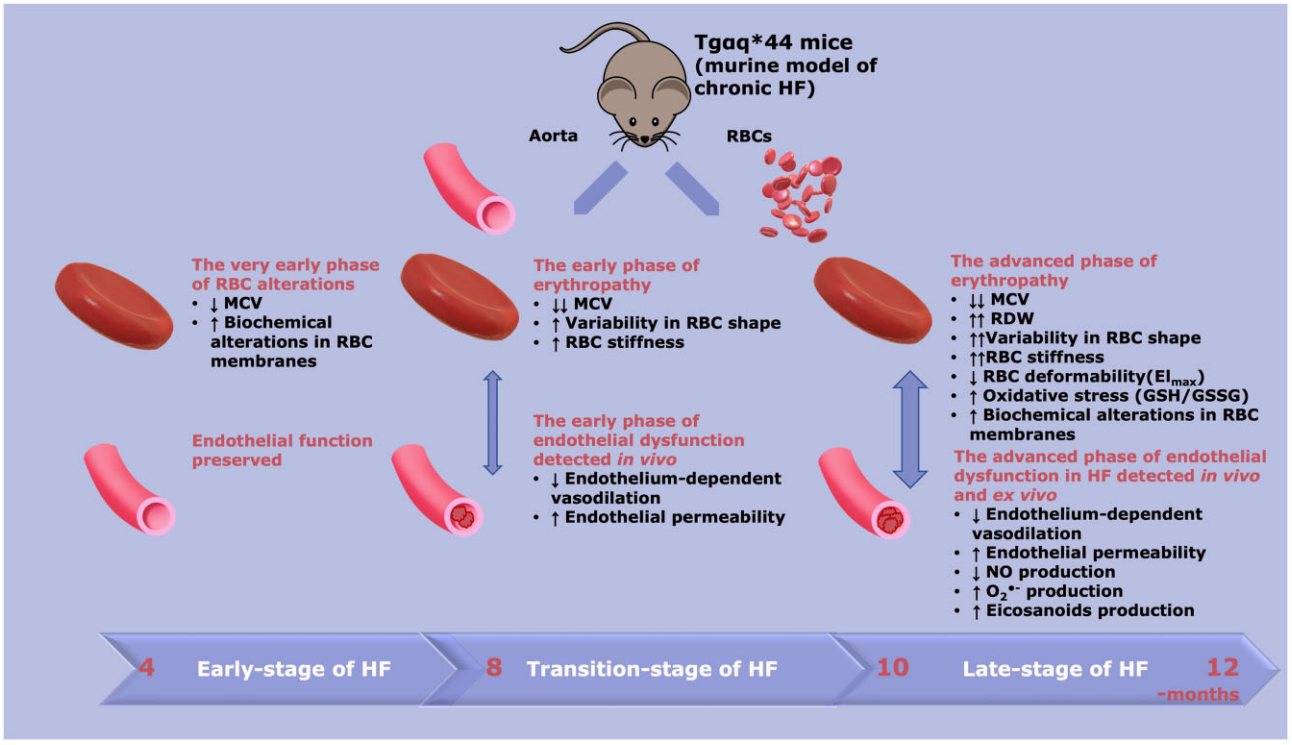

Figure 7 Schematic diagram summarizing the temporal relationship between the progression of endothelial dysfunction and erythropathy in Tgαq*44 mice, representing the murine model of chronic HF. At early stages of HF (4 months) a decrease in MCV ($P < 0.05$), biochemical alterations in RBC membranes [decreased phospholipids ($P < 0.0001$), and unsaturation ($P < 0.001$)] were present; however, these changes were not associated with functional alterations of RBCs and endothelial function was fully preserved. At the transition phase of HF, apart from a decrease in MCV ($P < 0.0001$), a substantial increase in RBC stiffness ($P < 0.0001$), and alteration in RBC shape were noted (early phase of erythropathy), as well as impaired endothelium-dependent vasodilation in the aorta and an increase in endothelial permeability ($P < 0.01$) (early phase of endothelial dysfunction). At the end stage of HF, a number of RBC indices were greatly altered, including MCV ($P < 0.0001$), RDW ($P < 0.05$), RBC shape ($P < 0.0001$), RBC deformability ($P < 0.01$), and oxidative stress (increased GSH/GSSG ratio, $P < 0.05$) (advanced phase of erythropathy), and were associated with an advanced phase of endothelial dysfunction, characterized not only by functionally impaired endothelium-dependent vasodilation and increased endothelial permeability ($P < 0.05$) but also impaired NO production ($P < 0.05$), increased superoxide anion ($O_2^{\bullet-}$) ($P < 0.05$), and increased eicosanoid ($P < 0.05$) production. HF, heart failure; MCV, mean corpuscular volume; NO, nitric oxide; RBC, red blood cell; RDW, red blood cell distribution width.

in late-stage HF in this model, the systemic NO bioavailability eventually fell substantially despite the activation of the nitrite reductive pathway.

Concomitantly, in 12-month-old Tgαq*44 mice, ED was characterized by increased generation of cyclooxygenase-derived eicosanoids, such as PGD_2 and PGI_2 (assessed as its metabolite 6-keto $PGF_{1\alpha}$), which may play a compensatory role.[50] In turn, increased vascular PGE_2 could contribute to vascular inflammation and ED.[37]

The comprehensive nature of RBC analysis based on the numerous methods, including AFM and vibrational spectroscopy, adapted in the present work allowed us to obtain unprecedented insight into structural, functional, nanomechanical, and biochemical changes in RBCs related to the progression of ED in HF. We demonstrated that RBCs displayed mild alterations as early as in 4 months old Tgαq*44 mice. These changes included a reduction in MCV, suggesting early RBC anisocytosis in HF; a slightly altered aspect ratio (assessed by AFM topography), indicating an early RBC shape alteration; and a decrease in phospholipid content and unsaturated lipids in RBC membranes (assessed by vibrational spectroscopy), implying early RBC membranes changes. Still, these changed did not result in statistically significant alterations in the nanomechanics or deformability of RBCs at this stage of HF. However, even at this HF stage, some RBCs displayed notable changes in elasticity. Notably, several parameters of erythropathy were significantly accentuated in 8-month-old Tgαq*44 mice, including structural changes (increased AFM-based aspect ratio indicative of the presence of ellipsoidal RBCs) and nanomechanical alterations (increased RBC elasticity modulus). In 12-month-old Tgαq*44 mice, HF-linked erythropathy was characterized not only by severely altered RBC shape and elasticity but also by increased RDW, impaired RBC deformability, and oxidative stress (GSH/GSSG ratio).

Taken together, in Tgαq*44 mice, HF-linked erythropathy was characterized by early detectable changes in RBC size and membrane composition but preserved RBC function, which could suggest early changes in erythropoiesis, most likely of a compensatory nature.[51] Then, with HF progression erythropathy involved altered shape and elasticity (AFM topography and nanoindentation), altered biochemical RBC homeostasis (oxidant stress), and, finally, impaired deformability of RBCs tested using the clinically used Rheoscan system (see *Figure* 7). Of note, alterations in RBC status based on Rheoscan, GSH/GSSG, and RDW parameters were detected at very late stages of erythropathy, in contrast to alterations in RBC membranes and changes in their nanomechanical profile detected in the early phase of HF. Interestingly, alterations in the

biochemical profile of RBC membranes and the size of RBCs shown here displayed a distinct pattern compared with atherosclerosis[40] or HF of ischaemic origin.[52] In a previous study by our group[40] using ApoE/LDLR$^{-/-}$ mice, phospholipids and unsaturated lipids decreased with the progression of atherosclerosis; however, the total lipid content and MCV was higher, without significant differences in RDW, in ApoE/LDLR$^{-/-}$ mice compared with age-matched controls. In the current study, levels of phospholipids and lipid unsaturation in RBC membranes were significantly lower even in the early phase of HF in 4- and 6-month-old Tgαq*44 mice, without changes in total lipid content. MCV values were reduced and further decreased with the progression of HF, whereas a significant increase in RDW values was observed in the late stage of HF in 12-month-old Tgαq*44 mice only. These results agree with the accepted notion that the modification of the lipid composition in the RBC membranes results in changes in their shape and elasticity. Furthermore, our results revealed that HF-related erythropathy displayed different types of RBC alterations compared with atherosclerosis-related changes.[40]

Most importantly, our results showed that HF-linked erythropathy in Tgαq*44 mice was temporally linked with the progression of ED. Moreover, the progression of erythropathy seems to be correlated with progressive impairment of endothelial function (alterations in RBC elasticity were correlated with progressive impairment of Ach-induced NO-dependent vasodilation in the aorta).

Of note, in 8-month-old Tgαq*44 mice, a severe pattern of HF-linked erythropathy was present. This stage of HF in Tgαq*44 mice was characterized by the presence of ED, whereas cardiac function was relatively compensated compared with late-stage HF in 12-month-old Tgαq*44 mice, which was characterized by severe impairment of basal cardiac function, cardiac reserve, and exercise capacity.[26] Taken together, our findings support the notion that endothelial function plays a key role in maintaining RBC haemostasis. As such, systemic ED may accelerate erythropathy. However, erythropathy has detrimental effects on endothelial function in other diseases.[19] This study also provided evidence supporting such a possibility. In advanced erythropathy, RBCs taken from 12-month-old Tgαq*44 mice and coincubated with isolated aorta rings induced impairment in endothelium-dependent relaxation in the *ex vivo* assay, and this effect was partially prevented by the inhibition of arginase. Of note, a similar experimental approach was previously used to show the contribution of diabetic erythropathy to the development of ED in diabetes.[53] Interestingly, Pernow *et al.*[19] discovered that the activation of arginase I in RBCs contributed to the development of ED in diabetes. Arginase in RBCs was also suggested to mediate ED associated with pre-eclampsia.[54]

Interestingly, in our study, ABH (an inhibitor of arginase types I and II) prevented RBC-induced impairment of endothelial function. This effect was, however, only detectable for the highest concentration of Ach. Pernow *et al.*[55] show that murine RBC expresses only arginase type I, but not arginase type II. Thus, our data suggest that impaired NO-dependent function in Tgaq*44 mice may be partially due to arginase I activity in RBC, but of course, this is just one of a number of mechanisms that could contribute to systemic ED in HF. Also, erythropathy could contribute to ED by mechanisms independent on arginase.[21,22,56–58]

Taken together, there seems to be a reciprocal relationship between endothelial function and RBC haemostasis in HF as suggested previously for diabetes.[19] Systemic ED accelerates erythropathy and vice versa, erythropathy may contribute to ED. These results suggest that erythropathy may be regarded as a marker and a mediator of systemic ED in HF. Furthermore, RBC arginase and possibly other RBC-mediated mechanisms may represent novel therapeutic targets for systemic ED in HF.

Previous studies showed that RBCs express functional eNOS protein, which is closely correlated with FMD in humans,[56] confirming a strong association between RBC functional status and endothelial function. Indeed, changes in RBC membranes could lead to increased RBC adhesion to endothelial cells;[19,57] for example, in diabetes, malaria, and haemoglobinopathies.[19] Increased RBC adhesion to the endothelium may lead to impaired tissue microcirculation.[21,22] Furthermore, amylin deposited on RBCs[58] or myeloperoxidase activation on the RBC surface could also contribute to oxidative stress and impairment of NO-dependent relaxation.[59] It remains to be established whether any of these RBC-mediated mechanisms also contribute to ED in HF. Moreover, previous studies of HF-linked erythropathy, defined as RDW, predicted a poor prognosis in patients with clinical HF.[17] Interestingly, it was suggested that HF-linked erythropathy was independent of systemic inflammation, kidney function, and numerous other studied variables, including NT-proBNP (a good biomarker of HF progression),[60] leaving the underlying mechanisms of the relationship between RDW and HF unclear.[17,18] In agreement with these findings in Tgaq*44 mice, systemic inflammation, erythropoietin, and kidney failure are also unlikely mechanisms of HF-linked erythropathy because the first two were not altered in 4-, 8-, and 12-month-old Tgαq*44 mice (results not shown) and the latter was a late phenomenon, as evidenced by the fact that the plasma urea concentration increased only in 12-month-old Tgaq*44 mice.

Our study has several limitations. As in previous work using this model,[24,27] only female mice were used, so we cannot be sure whether the findings of this work are also relevant to male Tgαq*44 mice. To confirm the detrimental effects of RBCs on endothelial function *ex vivo*, the isolated aorta was used similarly to in methodology described previously,[19] but we cannot be sure to what extent RBCs contribute to ED in HF *in vivo* since *ex vivo* studies are not able to fully mimic the *in vivo* setting. Finally, although we provided experimental evidence that RBCs in advanced erythropathy induce impaired endothelial function, and we postulated arginase in RBC to be partially involved, further experiments with more selective arginase inhibitors and tissue-specific arginase knock-out are mandatory to delineate in detail the importance of arginase in impaired NO-dependent function in Tgaq*44 mice.

In conclusion, HF-linked erythropathy in Tgaq*44 mice involved progressive alterations on functional, structural, nanomechanical, and biochemical levels. The temporal relationship and correlation between the progression of HF-linked erythropathy and the progression of impairment of vascular NO-dependent function in Tgαq*44 mice suggest that erythropathy may be a marker and a mediator of vascular dysfunction in HF. To the best of our knowledge, this relationship was not demonstrated previously in the context of HF, despite a wealth of evidence that RDW has prognostic significance in HF. Surprisingly, HF represents a disease in which targeting RBCs may represent a novel treatment modality to reverse systemic ED.

Authors' contributions

T.M.and S.C. conceived and designed the study. T.M., B.P., M.T.-K., A.Bar. A.K., K.B., A.W., A.Blat, K.M.-G., M.G., A.T., M.S., R.R.-D., K.W.-L., and A.Kubi performed experiments. T.M., B.P., M.T.-K., A.Bar, A.W., and A.Blat analysed the data. T.M. and M.T.-K. prepared the figures. T.M. and S.C. wrote the draft of the manuscript. K.M.M. and A.B. critically revised the manuscript for important intellectual content. K.M.M. edited and revised the manuscript. T.M. and S.C. wrote the final version of the manuscript. All authors read and approved the final version of the manuscript.

Conflict of interest: none declared.

Funding

This work was supported by the National Science Centre, Poland by PRELUDIUM 15 grant (no. UMO 2018/29/N/NZ4/02915 to T.M.) and partial by Team Tech–Core Facility program of the FNP (Foundation for Polish Science) co-financed by the European Union under the European Regional Development Fund (project No. POIR.04.04.00-00-5CAC/17–00 to S.C.) and an OPUS 12 grant (no. UMO 2016/23/B/ST4/00795 to K.M.M.).

Data availability

The data underlying this article are available on reasonable request to the corresponding author.

References

1. Cortese-Krott MM, Kelm M. Endothelial nitric oxide synthase in red blood cells: key to a new erythrocrine function? *Redox Biol* 2014;**2**:251–258.
2. Gevaert AB, Lemmens K, Vrints CJ, Van Craenenbroeck EM. Targeting endothelial function to treat heart failure with preserved ejection fraction: the promise of exercise training. *Oxid Med Cell Longev* 2017;**2017**:4865756.
3. Giannitsi S, Bougiakli M, Bechlioulis A, Naka K. Endothelial dysfunction and heart failure: a review of the existing bibliography with emphasis on flow mediated dilation. *JRSM Cardiovasc Dis* 2019;**8**:2048004019843047.
4. Baldus S, Köster R, Chumley P, Heitzer T, Rudolph V, Ostad MA, Warnholtz A, Staude HJ, Thuneke F, Koss K, Berger J, Meinertz T, Freeman BA, Münzel T. Oxypurinol improves coronary and peripheral endothelial function in patients with coronary artery disease. *Free Radic Biol Med* 2005;**39**:1184–1190.
5. Erbs S, Gielen S, Linke A, Möbius-Winkler S, Adams V, Baither Y, Schuler G, Hambrecht R. Improvement of peripheral endothelial dysfunction by acute vitamin C application: different effects in patients with coronary artery disease, ischemic, and dilated cardiomyopathy. *Am Heart J* 2003;**146**:280–285.
6. Zhang M, Perino A, Ghigo A, Hirsch E, Shah AM. NADPH oxidases in heart failure: poachers or gamekeepers? *Antioxid Redox Signal* 2013;**18**:1024–1041.
7. Bauersachs J, Widder JD. Endothelial dysfunction in heart failure. *Pharmacol Rep* 2008;**60**:119–126.
8. Schäfer A, Fraccarollo D, Tas P, Schmidt I, Ertl G, Bauersachs J. Endothelial dysfunction in congestive heart failure: ACE inhibition vs. angiotensin II antagonism. *Eur J Heart Fail* 2004;**6**:151–159.
9. Battault S, Meziat C, Nascimento A, Braud L, Gayrard S, Legros C, De Nardi F, Drai J, Cazorla O, Thireau J, Meyer G, Reboul C. Vascular endothelial function masks increased sympathetic vasopressor activity in rats with metabolic syndrome. *Am J Physiol Heart Circ Physiol* 2018;**314**:H497–H507.
10. Joannides R, Bizet-Nafeh C, Costentin A, Iacob M, Derumeaux G, Cribier A, Thuillez C. Chronic ACE inhibition enhances the endothelial control of arterial mechanics and flow-dependent vasodilatation in heart failure. *Hypertension* 2001;**38**:1446–1450.
11. Bauersachs J, Heck M, Fraccarollo D, Hildemann SK, Ertl G, Wehling M, Christ M. Addition of spironolactone to angiotensin-converting enzyme inhibition in heart failure improves endothelial vasomotor dysfunction: role of vascular superoxide anion formation and endothelial nitric oxide synthase expression. *J Am Coll Cardiol* 2002;**39**:351–358.
12. Hambrecht R, Fiehn E, Weigl C, Gielen S, Hamann C, Kaiser R, Yu J, Adams V, Niebauer J, Schuler G. Regular physical exercise corrects endothelial dysfunction and improves exercise capacity in patients with chronic heart failure. *Circulation* 1998;**98**:2709–2715.
13. Fischer D, Rossa S, Landmesser U, Spiekermann S, Engberding N, Hornig B, Drexler H. Endothelial dysfunction in patients with chronic heart failure is independently associated with increased incidence of hospitalization, cardiac transplantation, or death. *Eur Heart J* 2005;**26**:65–69.
14. Klosinska M, Rudzinski T, Grzelak P, Stefanczyk L, Drozdz J, Krzeminska-Pakula M. Endothelium-dependent and -independent vasodilation is more attenuated in ischaemic than in non-ischaemic heart failure. *Eur J Heart Fail* 2009;**11**:765–770.
15. Patel AR, Kuvin JT, Pandian NG, Smith JJ, Udelson JE, Mendelsohn ME, Konstam MA, Karas RH. Heart failure etiology affects peripheral vascular endothelial function after cardiac transplantation. *J Am Coll Cardiol* 2001;**37**:195–200.
16. Shah A, Gkaliagkousi E, Ritter JM, Ferro A. Endothelial function and arterial compliance are not impaired in subjects with heart failure of non-ischemic origin. *J Card Fail* 2010;**16**:114–120.
17. Borné Y, Smith JG, Melander O, Hedblad B, Engström G. Red cell distribution width and risk for first hospitalization due to heart failure: a population-based cohort study. *Eur J Heart Fail* 2011;**13**:1355–1361.
18. Pascual-Figal DA, Bonaque JC, Redondo B, Caro C, Manzano-Fernandez S, Sánchez-Mas J, Garrido IP, Valdes M. Red blood cell distribution width predicts long-term outcome regardless of anaemia status in acute heart failure patients. *Eur J Heart Fail* 2009;**11**:840–846.
19. Pernow J, Mahdi A, Yang J, Zhou Z. Red blood cell dysfunction: a new player in cardiovascular disease. *Cardiovasc Res* 2019;**115**:1596–1605.
20. Unruh D, Srinivasan R, Benson T, Haigh S, Coyle D, Batra N, Keil R, Sturm R, Blanco V, Palascak M, Franco RS, Tong W, Chatterjee T, Hui DY, Davidson WS, Aronow BJ, Kalfa T, Manka D, Peairs A, Blomkalns A, Fulton DJ, Brittain JE, Weintraub NL, Bogdanov VY. Red blood cell dysfunction induced by high-fat diet: potential implications for obesity-related atherosclerosis. *Circulation* 2015;**132**:1898–1908.
21. Anniss AM, Sparrow RL. Variable adhesion of different red blood cell products to activated vascular endothelium under flow conditions. *Am J Hematol* 2007;**82**:439–445.
22. Shiu YT, McIntire LV. In vitro studies of erythrocyte-vascular endothelium interactions. *Ann Biomed Eng* 2003;**31**:1299–1313.
23. Tikhomirova I, Petrochenko E, Muravyov A, Malysheva Y, Petrochenko A, Yakusevich V, Oslyakova A. Microcirculation and blood rheology abnormalities in chronic heart failure. *Clin Hemorheol Microcirc* 2017;**65**:383–391.
24. Mende U, Semsarian C, Martins DC, Kagen A, Duffy C, Schoen FJ, Neer EJ. Dilated cardiomyopathy in two transgenic mouse lines expressing activated G protein alpha(q): lack of correlation between phospholipase C activation and the phenotype. *J Mol Cell Cardiol* 2001;**33**:1477–1491.
25. Mackiewicz U, Czarnowska E, Brudek M, Pająk B, Duda M, Emanuel K, Csanyi G, Fedorowicz A, Grochal E, Tyrankiewicz U, Skórka T, Mende U, Lewartowski B, Chłopicki S. Preserved cardiomyocyte function and altered desmin pattern in transgenic mouse model of dilated cardiomyopathy. *J Mol Cell Cardiol* 2012;**52**:978–987.
26. Tyrankiewicz U, Olkowicz M, Skórka T, Jablonska M, Orzylowska A, Bar A, Gonet M, Berkowicz P, Jasinski K, Zoladz JA, Smolenski RT, Chlopicki S. Activation pattern of ACE2/Ang-(1-7) and ACE/Ang II pathway in course of heart failure assessed by multiparametric MRI in vivo in Tgαq44 mice. *J Appl Physiol (1985)* 2018;**124**:52–65.
27. Mende U, Kagen A, Cohen A, Aramburu J, Schoen FJ, Neer EJ. Transient cardiac expression of constitutively active Galphaq leads to hypertrophy and dilated cardiomyopathy by calcineurin-dependent and independent pathways. *Proc Natl Acad Sci U S A* 1998;**95**:13893–13898.
28. Bar A, Targosz-Korecka M, Suraj J, Proniewski B, Jasztal A, Marczyk B, Sternak M, Przybyło M, Kurpińska A, Walczak M, Kostogrys RB, Szymonski M, Chlopicki S. Degradation of glycocalyx and multiple manifestations of endothelial dysfunction coincide in the early phase of endothelial dysfunction before atherosclerotic plaque development in apolipoprotein e/low-density lipoprotein receptor-deficient mice. *J Am Heart Assoc* 2019;**8**:e011171.
29. Sternak M, Bar A, Adamski MG, Mohaissen T, Marczyk B, Kieronska A, Stojak M, Kus K, Tarjus A, Jaisser F, Chlopicki S. The deletion of endothelial sodium channel α (αENaC) impairs endothelium-dependent vasodilation and endothelial barrier integrity in endotoxemia. *Front Pharmacol* 2018;**9**:178.
30. Bar A, Skórka T, Jasiński K, Sternak M, Bartel Ż, Tyrankiewicz U, Chlopicki S. Retrospectively gated MRI for in vivo assessment of endothelium-dependent vasodilatation and endothelial permeability in murine models of endothelial dysfunction. *NMR Biomed* 2016;**29**:1088–1097.
31. Cheng HL, Wright GA. Rapid high-resolution T(1) mapping by variable flip angles: accurate and precise measurements in the presence of radiofrequency field inhomogeneity. *Magn Reson Med* 2006;**55**:566–574.
32. Wang J, Qiu M, Kim H, Constable RT. T1 measurements incorporating flip angle calibration and correction in vivo. *J Magn Reson* 2006;**182**:283–292.
33. Fedorowicz A, Buczek E, Mateuszuk Ł, Czarnowska E, Sitek B, Jasztal A, Chmura-Skirlińska A, Dib M, Steven S, Daiber A, Chlopicki S. Comparison of pulmonary and systemic NO- and PGI. *Oxid Med Cell Longev* 2018;**2018**:4036709.
34. Zhou Z, Mahdi A, Tratsiakovich Y, Zahorán S, Kövamees O, Nordin F, Uribe Gonzalez AE, Alvarsson M, Östenson CG, Andersson DC, Hedin U, Hermesz E, Lundberg JO, Yang J, Pernow J. Erythrocytes from patients with type 2 diabetes induce endothelial dysfunction via arginase I. *J Am Coll Cardiol* 2018;**72**:769–780.
35. Kij A, Kus K, Czyzynska-Cichon I, Chlopicki S, Walczak M. Development and validation of a rapid, specific and sensitive LC-MS/MS bioanalytical method for eicosanoid quantification—assessment of arachidonic acid metabolic pathway activity in hypertensive rats. *Biochimie* 2020;**171–172**:223–232.
36. Proniewski B, Kij A, Sitek B, Kelley EE, Chlopicki S. Multiorgan development of oxidative and nitrosative stress in LPS-induced endotoxemia in C57Bl/6 mice: DHE-based. *Oxid Med Cell Longev* 2019;**2019**:7838406.
37. Avendaño MS, García-Redondo AB, Zalba G, González-Amor M, Aguado A, Martínez-Revelles S, Beltrán LM, Camacho M, Cachofeiro V, Alonso MJ, Salaices M, Briones AM. mPGES-1 (microsomal prostaglandin e synthase-1) mediates vascular dysfunction in hypertension through oxidative stress. *Hypertension* 2018;**72**:492–502.
38. Przyborowski K, Proniewski B, Czarny J, Smeda M, Sitek B, Zakrzewska A, Zoladz JA, Chlopicki S. Vascular nitric oxide-superoxide balance and thrombus formation after acute exercise. *Med Sci Sports Exerc* 2018;**50**:1405–1412.
39. Frolow M, Drozdz A, Kowalewska A, Nizankowski R, Chlopicki S. Comprehensive assessment of vascular health in patients; towards endothelium-guided therapy. *Pharmacol Rep* 2015;**67**:786–792.
40. Dybas J, Bulat K, Blat A, Mohaissen T, Wajda A, Mardyla M, Kaczmarska M, Franczyk-Zarow M, Malek K, Chlopicki S, Marzec KM. Age-related and atherosclerosis-related erythropathy in ApoE/LDLR. *Biochim Biophys Acta Mol Basis Dis* 2020;**1866**:165972.
41. Hempe JM, Ory-Ascani J. Simultaneous analysis of reduced glutathione and glutathione disulfide by capillary zone electrophoresis. *Electrophoresis* 2014;**35**:967–971.

42. Blat A, Wiercigroch E, Smeda M, Wislocka A, Chlopicki S, Malek K. Fourier transform infrared spectroscopic signature of blood plasma in the progression of breast cancer with simultaneous metastasis to lungs. *J Biophotonics* 2019;**12**:e201900067.
43. Bar A, Kieronska-Rudek A, Proniewski B, Suraj-Prażmowska J, Czamara K, Marczyk B, Matyjaszczyk-Gwarda K, Jasztal A, Kuś E, Majka Z, Kaczor A, Kurpińska A, Walczak M, Pieterman EJ, Princen HMG, Chlopicki S. In vivo magnetic resonance imaging-based detection of heterogeneous endothelial response in thoracic and abdominal aorta to short-term high-fat diet ascribed to differences in perivascular adipose tissue in mice. *J Am Heart Assoc* 2020;**9**:e016929.
44. Elas M, Bielanska J, Pustelny K, Plonka PM, Drelicharz L, Skorka T, Tyrankiewicz U, Wozniak M, Heinze-Paluchowska S, Walski M, Wojnar L, Fortin D, Ventura-Clapier R, Chlopicki S. Detection of mitochondrial dysfunction by EPR technique in mouse model of dilated cardiomyopathy. *Free Radic Biol Med* 2008;**45**:321–328.
45. Maupoint J, Besnier M, Gomez E, Bouhzam N, Henry JP, Boyer O, Nicol L, Mulder P, Martinet J, Richard V. Selective vascular endothelial protection reduces cardiac dysfunction in chronic heart failure. *Circ Heart Fail* 2016;**9**:e002895.
46. Vercauteren M, Remy E, Devaux C, Dautreaux B, Henry JP, Bauer F, Mulder P, Hooft van Huijsduijnen R, Bombrun A, Thuillez C, Richard V. Improvement of peripheral endothelial dysfunction by protein tyrosine phosphatase inhibitors in heart failure. *Circulation* 2006;**114**:2498–2507.
47. Barton M, Cosentino F, Brandes RP, Moreau P, Shaw S, LüScher TF. Anatomic heterogeneity of vascular aging: role of nitric oxide and endothelin. *Hypertension* 1997;**30**:817–824.
48. Sallam NA, Laher I. Redox signaling and regional heterogeneity of endothelial dysfunction in *db/db* mice. *Int J Mol Sci* 2020;**21**:6147.
49. Liu Y, Bubolz AH, Mendoza S, Zhang DX, Gutterman DD. H2O2 is the transferrable factor mediating flow-induced dilation in human coronary arterioles. *Circ Res* 2011;**108**:566–573.
50. Félétou M, Huang Y, Vanhoutte PM. Endothelium-mediated control of vascular tone: COX-1 and COX-2 products. *Br J Pharmacol* 2011;**164**:894–912.
51. Semenza GL. Involvement of oxygen-sensing pathways in physiologic and pathologic erythropoiesis. *Blood* 2009;**114**:2015–2019.
52. Tang HY, Wang CH, Ho HY, Wu PT, Hung CL, Huang CY, Wu PR, Yeh YH, Cheng ML. Lipidomics reveals accumulation of the oxidized cholesterol in erythrocytes of heart failure patients. *Redox Biol* 2018;**14**:499–508.
53. Mahdi A, Jiao T, Tratsiakovich Y, Yang J, Östenson CG, Pernow J, Zhou Z. Altered purinergic receptor sensitivity in type 2 diabetes-associated endothelial dysfunction and Up_4A-mediated vascular contraction. *Int J Mol Sci* 2018;**19**:3942.
54. McCann Haworth SM, Zhuge Z, Nihlén C, Von Rosen MF, Weitzberg E, Lundberg JO, Krmar RT, Nasiell J, Carlström M. Red blood cells from patients with pre-eclampsia induce endothelial dysfunction. *J Hypertens* 2021;**39**:1628–1641.
55. Yang J, Gonon AT, Sjöquist PO, Lundberg JO, Pernow J. Arginase regulates red blood cell nitric oxide synthase and export of cardioprotective nitric oxide bioactivity. *Proc Natl Acad Sci U S A* 2013;**110**:15049–15054.
56. Verma N, Liu M, Ly H, Loria A, Campbell KS, Bush H, Kern PA, Jose PA, Taegtmeyer H, Bers DM, Despa S, Goldstein LB, Murray AJ, Despa F. Diabetic microcirculatory disturbances and pathologic erythropoiesis are provoked by deposition of amyloid-forming amylin in red blood cells and capillaries. *Kidney Int* 2020;**97**:143–155.
57. Adam M, Gajdova S, Kolarova H, Kubala L, Lau D, Geisler A, Ravekes T, Rudolph V, Tsao PS, Blankenberg S, Baldus S, Klinke A. Red blood cells serve as intravascular carriers of myeloperoxidase. *J Mol Cell Cardiol* 2014;**74**:353–363.
58. Helms CC, Gladwin MT, Db K-S. Erythrocytes and vascular function: oxygen and nitric oxide. *Front Physiol* 2018;**9**:125.
59. Cortese-Krott MM, Rodriguez-Mateos A, Sansone R, Kuhnle GG, Thasian-Sivarajah S, Krenz T, Horn P, Krisp C, Wolters D, Heiß C, Kröncke KD, Hogg N, Feelisch M, Kelm M. Human red blood cells at work: identification and visualization of erythrocytic eNOS activity in health and disease. *Blood* 2012;**120**:4229–4237.
60. Argan O, Ural D, Karauzum K, Bozyel S, Aktaş M, Karauzum I, Kozdag G, Agacdiken Agir A. Elevated levels of vitamin B12 in chronic stable heart failure: a marker for subclinical liver damage and impaired prognosis. *Ther Clin Risk Manag* 2018;**14**:1067–1073.

Translational perspective

Endothelial dysfunction (ED) and red blood cell (RBC) distribution width both have prognostic value for heart failure (HF), but it is not known whether these pathologies are related. We comprehensively characterized endothelial and RBC functional status in a unique murine model of chronic HF with a prolonged time course of HF progression. Our results suggest that ED accelerates erythropathy and, conversely, erythropathy may contribute to ED. Accordingly, erythropathy in HF reflects ED and involves various changes (in functional, structural, nanomechanical, and biochemical levels) that could have diagnostic and therapeutic significance for HF.